Measurements of rare Higgs decay couplings at the FCC-hh

Birgit Stapf[1*], Michele Selvaggi[1*] and Jan Eysermans[2*]

[1]CERN, Geneva, Switzerland.
[2]Massachusetts Institute of Technology, Cambridge, USA.

*Corresponding author(s). E-mail(s): birgit.stapf@cern.ch; michele.selvaggi@cern.ch; jan.eysermans@cern.ch;

1 Introduction

Measurements of the Higgs bosons properties, such as of its couplings with other Standard Model (SM) particles, at the Future Circular Collider(FCC) will allow to further understand its role in the SM and thereby in our universe. While the prospects for Higgs studies at the HL-LHC as well as the FCC-ee will already advance current levels of precision and insight significantly [1], [2], the hadron-hadron collider phase FCC-hh is crucial to complete the picture, by enabling high precision measurements of Higgs processes that remain out of reach for the nearer future. An example are the measurements of its couplings in rare decay modes, such as $H \rightarrow \mu\mu$, $H \rightarrow \gamma\gamma$ and $H \rightarrow Z\gamma$, which will be statistically limited at the FCC-ee. A previous study of these Higgs decay modes was performed as part of the Conceptual Design Report (CDR) [3, 4] of the FCC-hh and detailed in Ref. [5], assuming the CDR baseline operation at $\sqrt{s}=$ 100 TeV and an integrated luminosity of 30 ab^{-1}. This study focused on analyzing Higgs production at large transverse momenta, p_{T}^{H} , exploiting the fact that with the expected FCC-hh dataset even this region of phase space will be abundantly populated, and that experimental uncertainties in this region are typically smaller than at lower p_{T}^{H} , where reconstruction of physics objects is more difficult due to e.g. trigger thresholds or the impact of pile-up. In order to keep the projections robust and largely independent of assumptions on the levels of theoretical (and to some extent experimental) uncertainties in the future, measurements of Higgs decay channels within similar fiducial regions were combined into a measurement of the production ratio. Common theoretical uncertainties regarding the production cross-section, as well as experimental uncertainties deriving from the luminosity measurement, vanish in such a ratio. In this way, sub-percent level precision on the Higgs couplings in the $H \to \mu\mu$, $H \to \gamma\gamma$ and $H \to Z\gamma$ decay channels with CDR baseline FCC-hh scenario were achieved.

This note presents on update to these Higgs boson studies in rare decay modes at the FCC-hh. As a first case study, the measurement of the Higgs to muon coupling exploiting the ratio of $H \to \mu\mu$ over $H \to ZZ* \to 4\mu$ production is revisited for the updated FCC-hh baseline scenario, which assumes an integrated luminosity of 30 ab^{-1} at a center-of-mass energy of $\sqrt{s}$ = 84 TeV. While the previous results were obtained from a simple counting experiment, the new strategy exploits the different shapes of the $m_{\mu\mu}$ invariant mass and $p_{T,\mu\mu}$ distributions between signal and background in a 2D template fit. Moreover the estimation of the experimental systematic uncertainties was further refined, using p_T-dependent scale factors capturing the reconstruction efficiency uncertainties of each muon, and measuring the non-resonant background in a data-driven way from the large statistics in the sidebands.

In addition, several alternative operating scenarios for the FCC-hh in contrast to the CDR baseline idea of a dataset of 30ab^{-1} at 100 TeV center of mass energy have come under discussion during the drafting process of the FCC feasibility study report (FSR) [6–8]. The main limiting factor defining the different scenarios is the necessary dipole magnet strength. Detailed descriptions of these scenarios are given in Ref. [9], while Table 1 summarizes only the key parameters relevant for the physics studies here. Updated results of the Higgs to muon couplings analysis are provided for the four different scenarios listed in the table.

Scenario	FSR baseline	CDR baseline	F12PU	F20
$\sqrt{s}$ in TeV	84	100	72	120
Peak arc dipole field in T	14	16	12	20
Pile-up	590	950	950	141
Total int. luminosity in ab^{-1}	30	30	42	12

Table 1: Key parameters of the possible FCC-hh operating scenarios studied in this note. The total integrated luminosities for the F12PU and F20 scenario are derived by rescaling the baseline 30ab^{-1} with the relative fraction of achievable luminosity per year over the baseline in each case. Details on the corresponding accelerator design parameters can be found in Ref. [9] and Ref. [4].

Completion of this update by expanding the newly defined, more sensitive analysis strategy also to the $H \to \gamma\gamma$ and $H \to Z\gamma$ channels is expected within the coming months.

2 Event generation

The analysis relies on Monte Carlo generated events for both the signal and the background processes considered. In general, all samples are generated at leading-order (LO) precision using `MadGraph5_aMC@NLO` [10] with `NNPDF3.0NLO` [11]. `Pythia8` [12] is used for the Higgs boson decay into two photons, parton showering, and hadronization effects. Since the analysis aims to exploit the large statistics of events with large transverse momentum of the Higgs to di-photon candidate, the generation of signal and dominant background processes accounts for additional jets in the matrix element, as specified in the following. The matching between matrix element and parton shower jets employed follows the MLM-scheme described in Ref. [13].

For the Higgs boson signal, its leading production modes of gluon-gluon fusion (ggH), vectorboson fusion (VBF H), top-quark pair associated production ($t\bar{t}H$) and the production in association with a vector boson (VH), are considered. The event generation of ggH and VH events includes contributions up-to and including two additional jets in the matrix element, while that of VBF H and $t\bar{t}H$ events considers only up to one additional jet. For each production mode the respective LO cross-section is corrected to higher orders using k-factors derived from the most accurate predictions in Ref. [14] for the studies at 100 TeV. These k-factors are thus assumed to be independent of the center of mass energy.

In terms of background, only the dominant continuum backgrounds processes are considered: that is the $\mu\mu$ continuum in the $H \to \mu\mu$ analysis, and the 4ℓ continuum in the $H \to ZZ* \to 4\mu$ analysis. The generation of the former includes up to two additional MLM-matched jets in the matrix element, while the latter stops at one additional MLM-matched jet. In both cases, an invariant mass of the Higgs boson candidate in the range of $50 < m^{\text{gen}}_{\mu\mu\,\text{or}\,4\mu} < 200$ GeV is required at generator level, in order to increase MC statistics in the phase space region of interest for the analysis. The LO $\mu\mu$ continuum cross-section is corrected with a k-factor of 1.2 following Ref. [5] and that of the 4ℓ continuum with a k-factor of 1.6 extracted from the predictions in Ref. [15]. Again, these k-factors were evaluated using the 100 TeV cross-sections. Background contributions from mis-identified objects (fakes) were not considered in the analysis.

Table 2 summarizes the respective cross-sections of each signal and background process considered, for the various center of mass energies studied, including all correction-factors as discussed above.

Process	Cross-section in pb, for $\sqrt{s}$ = 72 TeV	84 TeV	100 TeV	120 TeV
Signals				
ggH	543	657	802	999
VBF H	45	54	69	86
$t\bar{t}H$	19	25	33	45
VH	19	22	27	32
Backgrounds				
$\mu\mu$ continuum	257	288	339	385
4ℓ continuum	0.050	0.056	0.064	0.073

Table 2: Overview of total signal and background cross-sections at different center of mass energies. The background cross-sections refer to the fiducial region, with $50 < m^{\text{gen}}_{\mu\mu\,\text{or}\,4\mu} < 200$ GeV.

3 Event Reconstruction and Selection

A reference detector for the FCC-hh has been designed and described in the CDR. All samples considered in this analysis rely on a fast simulation of this detector design with the DELPHES tool [16], which describes the response of the detector components using parameterizations of the resolution and efficiency functions. Details on the specific assumptions and parameterizations for the FCC-hh reference detector scenario can be found in Ref. [17], while Ref. [16] describes the generalities of object reconstruction in DELPHES. The muons as used in this analysis, are reconstructed with a relative momentum resolution of the percent-level, and an efficiency ranging from 90-97%. Although no direct pile-up overlay is considered in the fast simulations performed here, the impact of pile-up at LHC levels is implicitly included through the DELPHES parameterizations.

For the technical implementation of the event generation and simulation, the common software stack for future facilities provided by the KEY4HEP framework [18, 19] is employed. In particular, the samples used here are in EDM4HEP format [20]. The complete list of generated samples can be found in Ref. [21]. The samples are further processed with the FCCANALYSES framework [22], implementing the selection of final state objects and events based on the criteria outlined in Table 3.

	$H \to \mu\mu$	$H \to ZZ* \to 4\mu$
Muon transverse momenta	$p_{\mathrm{T}}(\mu_1) > 20$ GeV $p_{\mathrm{T}}(\mu_2) > 20$ GeV	$p_{\mathrm{T}}(\mu_1) > 20$ GeV $p_{\mathrm{T}}(\mu_2) > 10$ GeV $p_{\mathrm{T}}(\mu_3) > 7$ GeV $p_{\mathrm{T}}(\mu_3) > 5$ GeV
Muon pseudorapidity	$\lvert\eta(\mu)\rvert < 4$	$\lvert\eta(\mu)\rvert < 4$
Muon isolation	rel. Iso. $(\mu) < 0.2$	rel. Iso. $(\mu) < 0.2$
Z decay candidates	-	$40 < m_{\mu\mu}$ (leading pair) < 120 GeV $12 < m_{\mu\mu}$ (subleading pair) < 120 GeV
Higgs candidate p_{T}	$p_{\mathrm{T}}^{\mu\mu} > 50$ GeV	$p_{\mathrm{T}}^{4\mu} > 50$ GeV

Table 3: Summary of object and event selection criteria per analysis.

4 Analysis strategy and systematic uncertainties

The selected events are further split into different regions of the transverse momentum of the Higgs candidate, $p_{\mathrm{T}}^{\mu\mu}$ and $p_{\mathrm{T}}^{4\mu}$ for the $H \to \mu\mu$ and $H \to ZZ* \to 4\mu$ analysis respectively. A template fit to the invariant mass of the Higgs candidate, $m_{\mu\mu}$ or $m_{4\mu}$ is then performed in each bin, in order to extract the $H \to \mu\mu$ and $H \to ZZ* \to 4\mu$ signal strengths. This differential measurement approach enhances the sensitivity of the analysis, as it exploits variations in the signal-to-background ratio across p_{T} regions, with higher p_{T} regions generally offering improved separation between signal and background. Moreover, it allows for better control of systematic uncertainties, since low p_T bins benefit from larger statistics than high p_T bins, but suffer from larger systematic uncertainties than high p_T bins.

The estimation of these systematic uncertainties is performed as follows:

Signal uncertainties

In each bin, a systematic uncertainty to account for the muon reconstruction efficiencies is determined from the parametrization first introduced in Ref. [5] and shown in Figure 1a and the Higgs signal. The corresponding relative uncertainty value per muon is taken from this parametrization depending on its transverse momentum, and an overall scalefactor for the event is defined as the multiplication of the individual muon uncertainty scalefactors. A normalization uncertainty, averaging across all events in the bin, is then determined from reweighting the invariant mass distributions in each bin with the scalefactor and comparing to the nominal case. Figure 1b shows the value of this muon reconstruction efficiency systematic per bin for each analysis. To illustrate the procedure, Figure 1c compares the distributions of the transverse momentum of the leading muon in the $H \to \mu\mu$ and $H \to ZZ* \to 4\mu$ analysis in an example p_T bin. The resulting scalefactor, shown in Figure 1d, is larger in the $H \to ZZ* \to 4\mu$ case, not only due to the higher muon multiplicity but also since the muons in $H \to ZZ* \to 4\mu$ decays exhibit lower p_T than those in $H \to \mu\mu$ decays for this very reason. In the template fit, the muon reconstruction efficiency uncertainty is described by a single nuisance parameter, therefore correlating the measurements across all p_T bins as well as between the $H \to \mu\mu$ and $H \to ZZ* \to 4\mu$ analysis. This gives a conservative estimate of the achievable sensitivity.

Additionally, a flat normalization uncertainty of 1% due the luminosity measurement is applied to the signals. This impacts only the standalone results of the $H \to \mu\mu$ and $H \to ZZ* \to 4\mu$ analyses, since in the ratio of $H \to \mu\mu$ over $H \to ZZ* \to 4\mu$ it cancels fully.

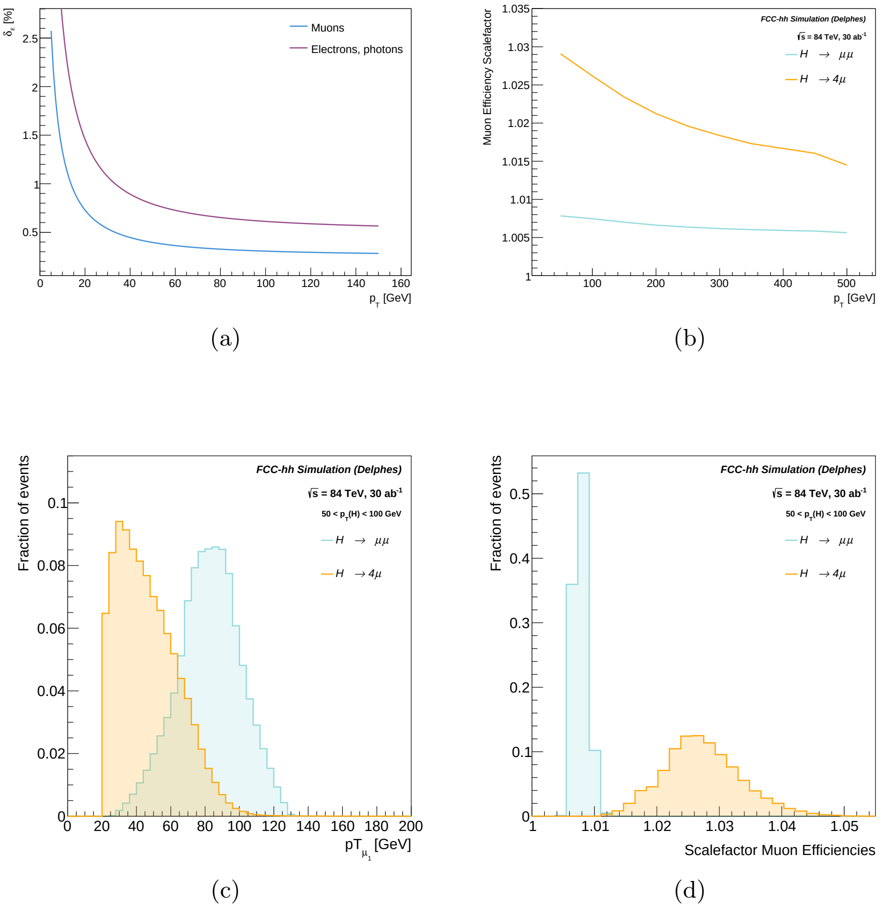

Fig. 1: Estimation of systematic uncertainties relating to object reconstruction efficiencies: (a) Parameterization of the assumed object reconstruction efficiencies as a function of the objects' transverse momentum, p_{T} , (b) evolution of the resulting overall scalefactor in the $H \rightarrow \mu\mu$ and $H \rightarrow ZZ* \rightarrow 4\mu$ analyses across the p_{T} bins (c) example distributions of the leading muons transverse momentum in $H \rightarrow \mu\mu$ and $H \rightarrow ZZ* \rightarrow 4\mu$ events and the bin where $50 < p_{\mathrm{T}}^{H} < 100$ GeV and (d) the distribution of the muon efficiency uncertainty scalefactor per event in the same p_{T}^{H} bin. Here the "up" variation of the scalefactor is shown.

Background uncertainties

As the background normalization can be determined from the data sidebands with high precision, no further uncertainties on the background processes are assumed. Instead, a free floating normalization factor for each background is used in the fit. In the $H \rightarrow \mu\mu$ analysis region the uncertainty on the $\mu\mu$ continuum background normalization factor is constrained down to the sub-per-mille level, while in the $H \to ZZ* \to 4\mu$ analysis region the resulting 4ℓ continuum normalization uncertainty is approximately 1 per-cent.

Invariant mass distributions

Figures 2 and 3 show the resulting (pre-fit) distributions of the invariant mass of the Higgs candidate for signals and background in the different bins of p_{T}^{H} for the $H \to \mu\mu$ and $H \to ZZ* \to 4\mu$ analysis respectively. The relative signal systematic uncertainty bands determined as described above are shown in the bottom panel in each case: While the solid area indicates the total signal uncertainty combining the flat luminosity uncertainty with the p_{T} dependent uncertainty accounting for the muon reconstruction efficiency, the dashed area shows only the latter.

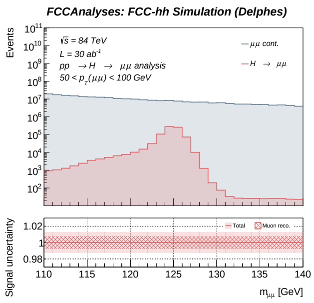

(a) $50 \leq p_T^{\mu\mu} < 100$ GeV

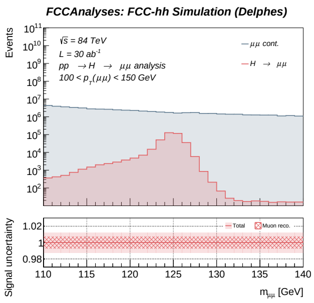

(b) $100 \leq p_T^{\mu\mu} < 150$ GeV

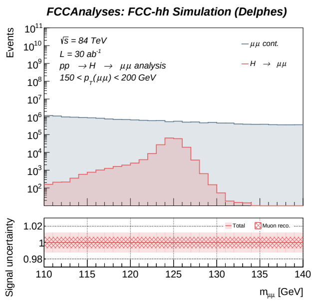

(c) $150 \leq p_T^{\mu\mu} < 200$ GeV

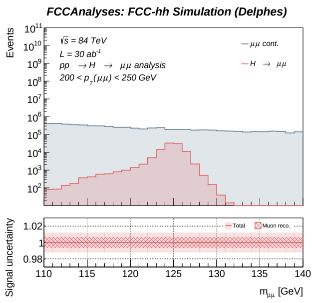

(d) $200 \leq p_T^{\mu\mu} < 250$ GeV

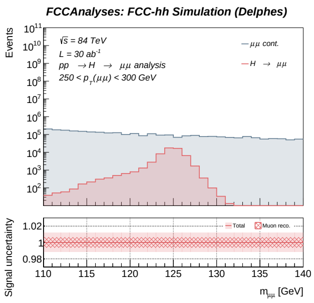

(e) $250 \leq p_T^{\mu\mu} < 300$ GeV

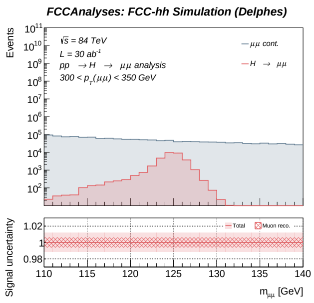

(f) $300 \leq p_T^{\mu\mu} < 350$ GeV

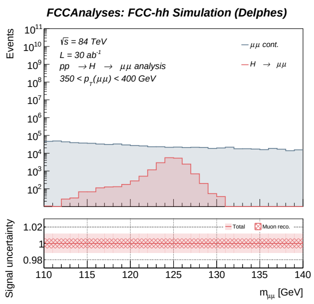

(g) $350 \leq p_T^{\mu\mu} < 400$ GeV

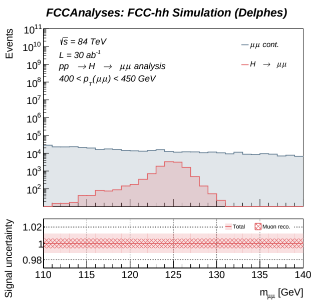

(h) $400 \leq p_T^{\mu\mu} < 450$ GeV

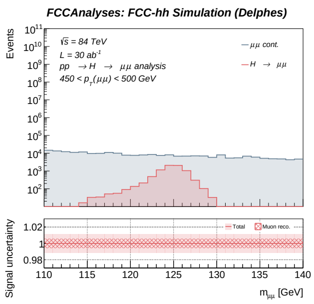

(i) $450 \leq p_T^{\mu\mu} < 500$ GeV

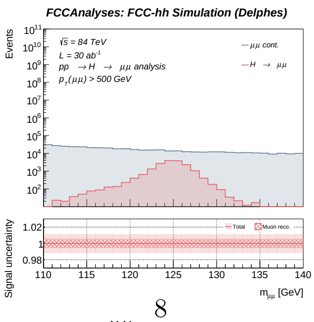

(j) $p_T^{\mu\mu} > 500$ GeV

Fig. 2: $H \to \mu\mu$ analysis: Distributions of $m_{\mu\mu}$ for the Higgs signals (red) and the $\mu\mu$ continuum background (blue), in the different bins of $p_T^{\mu\mu}$. The bottom panel indicates the relative signal systematic uncertainties.

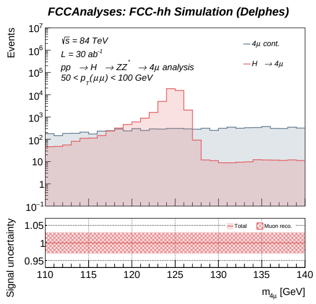

(a) $50 \leq p_T^{4\mu} < 100$ GeV

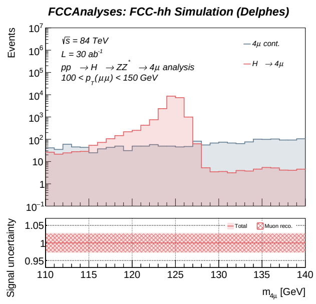

(b) $100 \leq p_T^{4\mu} < 150$ GeV

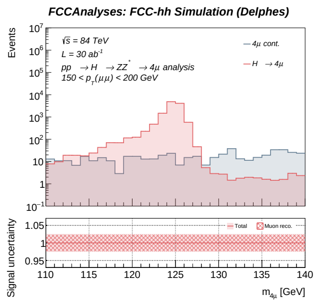

(c) $150 \leq p_T^{4\mu} < 200$ GeV

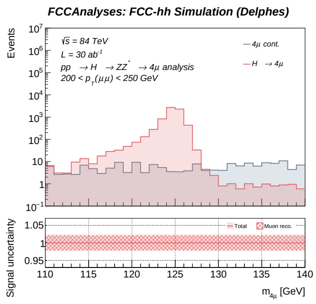

(d) $200 \leq p_T^{4\mu} < 250$ GeV

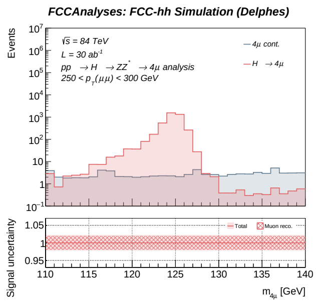

(e) $250 \leq p_T^{4\mu} < 300$ GeV

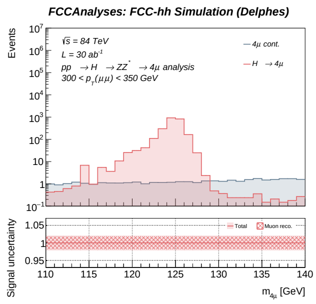

(f) $300 \leq p_T^{4\mu} < 350$ GeV

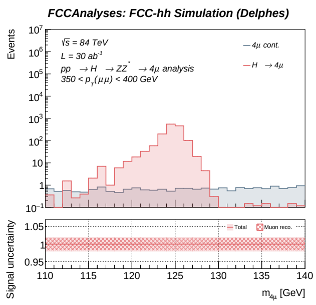

(g) $350 \leq p_T^{4\mu} < 400$ GeV

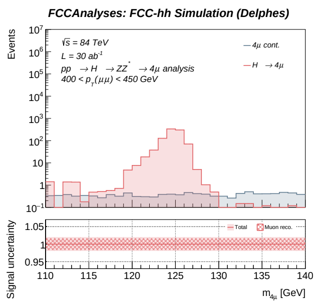

(h) $400 \leq p_T^{4\mu} < 450$ GeV

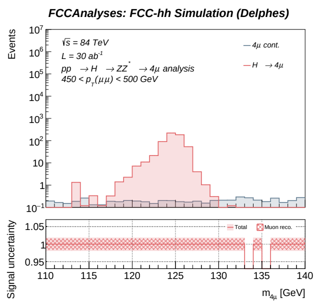

(i) $450 \leq p_T^{4\mu} < 500$ GeV

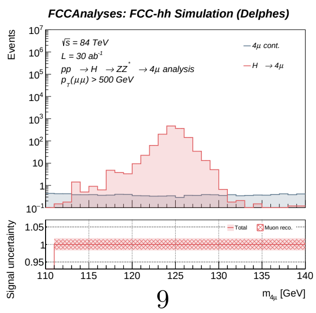

(j) $p_T^{4\mu} > 500$ GeV

Fig. 3: $H \to ZZ* \to 4\mu$ analysis: Distributions of $m_{4\mu}$ for the Higgs signals (red) and the 4ℓ continuum background (blue), in the different bins of $p_T^{4\mu}$. The bottom panel indicates the relative signal systematic uncertainties.

5 Results

Figure 4 shows the results of a differential measurement of the ratio $\mathcal{B}(\mathrm{H} \to \mu\mu)/\mathcal{B}(\mathrm{H} \to \mu\mu\mu\mu)$ in different ranges of the transverse momentum of the Higgs candidate, $\mathrm{p_T(H)}$, for the FSR baseline scenario of 84 TeV. Here, we use the same projection for the total integrated luminosity of 30 ab^{-1} as in the original CDR baseline, to be collected over the full lifetime across different experiments. Clearly, the binning in $\mathrm{p_T(H)}$ can be further optimized. But in this first iteration it serves well as a proof-of-concept, highlighting the key idea behind the FCC-hh measurements: that in phase space regions with higher transverse momentum of the Higgs candidate, the impact of the experimental uncertainties become smaller, and this benefit outweighs the loss in precision to due loss of available statistics. Indeed, when considering only a single bin in $\mathrm{p_T(H)}$, there is an optimum point for the achievable precision between 100 to 250 GeV, much the same as was found in the previous studies in Ref. [5]. Of course, the best sensitivity is achieved in the simultaneous fit across all $\mathrm{p_T(H)}$ bins reported in the bottom line of Figure 4, since the strength of each bin is fully exploited in this case. Here, we want to note that the $\mathrm{p_T}$-dependent uncertainty on the muon reconstruction is fully correlated across all bins in the simultaneous fit. This provides a conservative projection of the precision, since when de-correlating it into individual uncertainties that affect only a single bin each, the large size of the dataset leads to large constraints on the associated nuisance parameters.

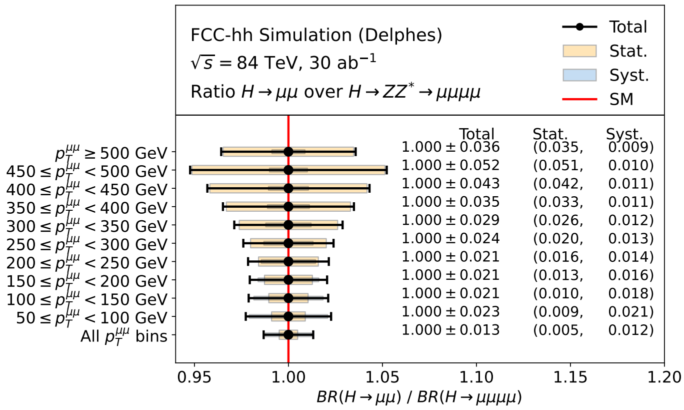

Fig. 4: Differential measurements of the ratio $\mathcal{B}(\mathrm{H} \to \mu\mu)/\mathcal{B}(\mathrm{H} \to \mu\mu\mu\mu)$ for different values of $\mathrm{p_T(H)}$ and the different operating scenarios.

Comparing the updated results further to those reported in Ref. [5], the new analysis strategy is both more realistic, as well as (slightly) more sensitive: Where the previous analysis discarded a significant fraction of the dataset by placing a high threshold on the minimum $\mathrm{p_T(H)}$, the simultaneous but differential fit exploits more of the dataset. Moreover, in the previous study only the events in a fixed window of 1 GeV width around the Higgs mass were considered. The invariant mass resolution is however dependent on the $p_T(H)$, an effect which is much better captured in the template fit across the larger mass range as performed here. Last, in the previous study the impact of the muon reconstruction uncertainty was averaged across the p_T in a given bin, while here it is fully evaluated event by event in the given bin.

The results of this improved strategy employing a differential, simultaneous template fit of the invariant mass spectra in different $p_T(H)$ bins in the four different energy and luminosity scenarios for the FCC-hh as discussed above are compared in Figure 5. Since the analysis is systematically dominated, the achievable precision is very similar across all scenarios - in each case the ratio of signal strengths can be measured down to the percent level. In particular, the results for the CDR baseline of 100 TeV are only roughly a per-mill better compared to the new FSR baseline scenario with a reduced energy of 84 TeV. Due to the smaller size of the dataset assumed for the 120 TeV scenario, this scenario provides the least sensitive results, while the impact of the lower center of mass energy in the 72 TeV scenario is fully compensated by the increase in integrated luminosity. It should be noted that we have assumed the same parametrization of the muon reconstruction uncertainty in all four scenarios studied here - an assumption that may not be warranted, given e.g. the different levels of pile-up for each case, as reported in Table 1. Further refinement of the systematic uncertainties under this aspect would be beneficial, however it is difficult to estimate the change of reconstruction uncertainties for such high levels of pile-ups (where we have to extrapolate quite far away to, from LHC experience) for a project so far in the future, which may employ advanced detector design and methods for pile-up suppression. We want to therefore stress again, that measuring ratios of Higgs signal strengths, allows to limit the impact of these kind of assumptions: in the $H \to \mu\mu$ over $H \to ZZ* \to 4\mu$ measurement the muon reconstruction systematic uncertainty cancels only partially, while which value is assumed exactly for the overall luminosity uncertainty has no impact on the precision, as this common uncertainty vanishes fully in the ratio.

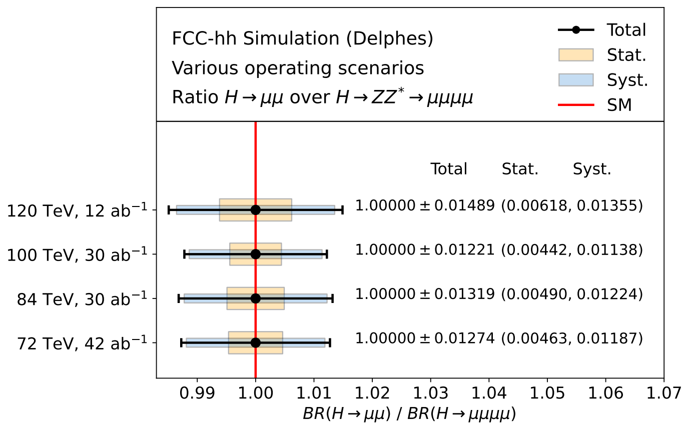

Fig. 5: Comparison of the best precision achieved from a differential measurement of the ratio $\mathcal{B}(H \to \mu\mu)/\mathcal{B}(H \to \mu\mu\mu\mu)$ between different FCC-hh operating scenarios.

$\sqrt{s}$ Scenario Int. lumi in ab^{-1}	84 TeV FSR baseline 30	100 TeV CDR baseline 30	72 TeV F12PU 42	120 TeV F20 12
$\delta g_{\text{H}\mu\mu}/g_{\text{H}\mu\mu}$ in %	0.660	0.611	0.637	0.745

Table 4: Comparison of the precision on absolute coupling strengths as inferred from the ratio analyses, for the four different FCC-hh operating scenarios.

A further benefit of the ratio measurement is that it allows to translate the relative coupling measurements of the FCC-hh to an absolute coupling measurement: in the full integrated FCC program, the branching ratio of Higgs to Z boson decays, $\mathcal{B}(H \to ZZ^*)$, will be measured so precisely in the FCC-ee phase that all relative measurements that involve the $H \to ZZ^*$ coupling in the denominator can be converted to absolute measurements of the branching fraction involved in the numerator. The (naive) translations into the achievable precision on the absolute couplings strength to muons, $\delta g_{\text{H}\mu\mu}/g_{\text{H}\mu\mu}$, from the ratio results reported in Figure 5 are given in Table 4. As can be seen, the results of the updated analyses confirm that a sub-percent level precision measurement of the Higgs to muon coupling will be achievable with the FCC.

As supplementary material to the results discussed in detail in this section, Appendix A.1 shows the full differential measurements of the $H \to \mu\mu$ over $H \to ZZ* \to 4\mu$ ratio for each of the four different operating scenarios studied, while Appendices A.2 and A.3 show the same results for the standalone $H \to \mu\mu$ and $H \to ZZ* \to 4\mu$ analyses respectively.

6 Conclusion

In this study, we revisited the prospects for precision measurements in rare decay modes of the Higgs boson at the FCC-hh, performing a differential measurement with respect to the transverse momentum of the Higgs candidate. By analyzing the ratio of $H \to \mu\mu$ over $H \to ZZ* \to 4\mu$ signal strengths, we demonstrated that this ratio is largely independent of common theoretical and experimental uncertainties, such as on the production cross-section and the luminosity, which cancel out in the ratio. Our findings show that a precision on the ratio of signal strengths of 1.32% can be achieved, which (naively) translates to a precision on the absolute coupling of the Higgs boson to muons of 0.66% , for the FSR baseline operating scenario of 30 ab^{-1} at a center of mass energy of 84 TeV.

Furthermore, we compared these results across four different operating scenarios, that have been under discussion for the FCC-hh: the CDR baseline of 30 ab^{-1} at 100 TeV, a lower energy scenario at 72 TeV with slightly larger integrated luminosity of 42 ab^{-1}, and a smaller dataset of 12 ab^{-1} at a higher energy of 120 TeV. The impact on the achievable precision on the Higgs to muon coupling was found to be minimal, as the analysis is primarily limited by systematic uncertainties, which we have assumed to be the same between the different scenarios. Further study of this may be of merit, as for example the levels of pile-up vary significantly between the different operating scenarios as well.

This analysis highlights the robustness of the $H \to \mu\mu$ to $H \to ZZ* \to 4\mu$ decay ratio as a tool for precise measurements of the Higgs boson's coupling to muons, with the FCC-hh offering promising prospects for advancing our understanding of Higgs physics, by allowing insight into rare Higgs decay processes that will remain statistically limited with collider projects in the nearer future such as the HL-LHC and the FCC-ee, and therefore only measured with limited precision. In this way, precision Higgs measurements at the FCC-hh are complementary to those at FCC-ee, underscoring the strength of the full integrated FCC program.

A Appendix

A.1 Results of the $H \to \mu\mu$ over $H \to ZZ* \to 4\mu$ ratio analysis for various operating scenarios

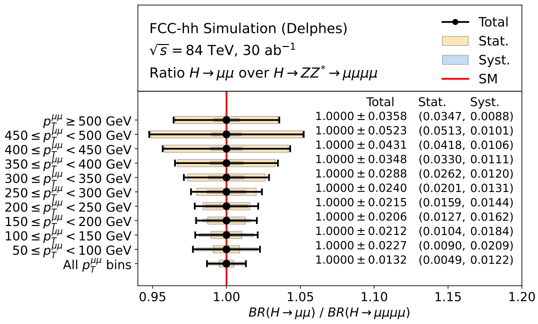

(a) FSR baseline of 84 TeV

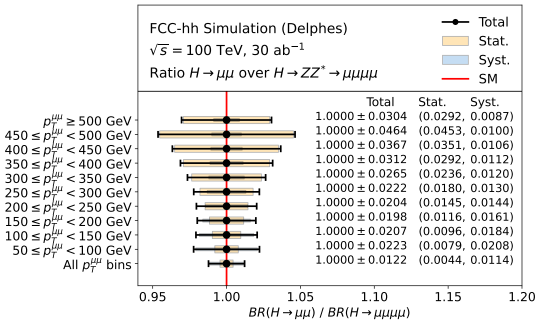

(b) CDR baseline of 100 TeV

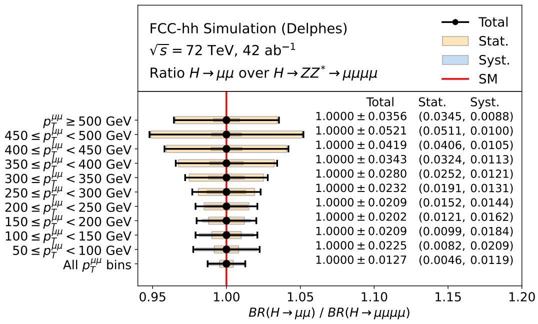

(c) F12PU scenario with 72 TeV

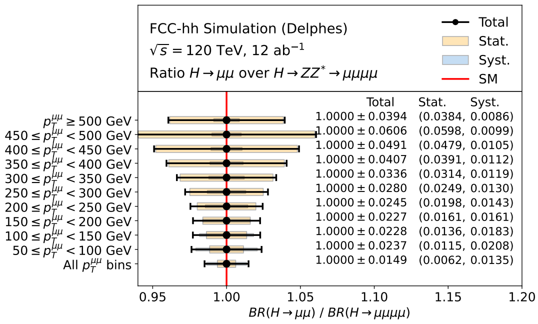

(d) F20 scenario with 120 TeV

Fig. A.1: Differential measurements of the ratio $\mathcal{B}(\mathrm{H} \to \mu\mu)/\mathcal{B}(\mathrm{H} \to \mu\mu\mu\mu)$ for different values of $\mathrm{p_T(H)}$ and the different FCC-hh operating scenarios.

A.2 Standalone results of the $H \to \mu\mu$ analysis

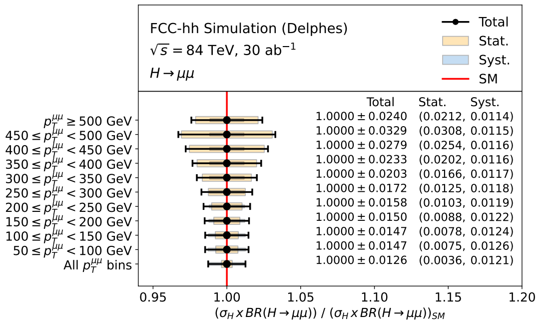

(a) FSR baseline of 84 TeV

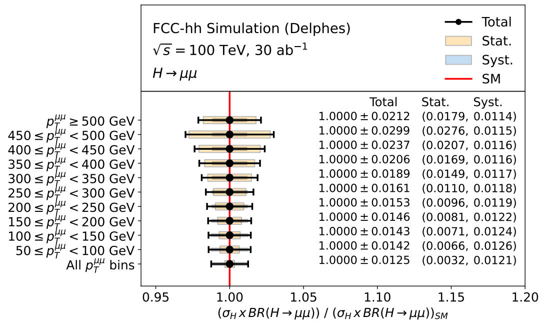

(b) CDR baseline of 100 TeV

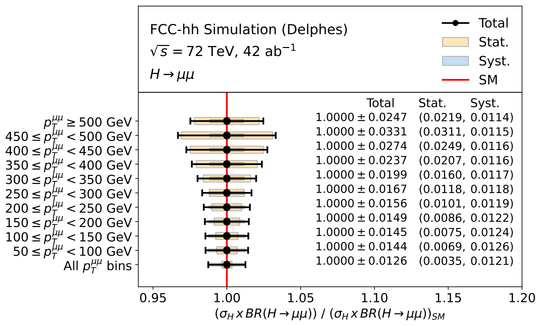

(c) F12PU scenario with 72 TeV

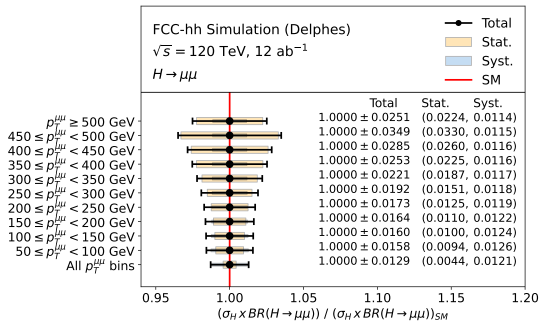

(d) F20 scenario with 120 TeV

Fig. A.2: Differential measurements of the signal strength $\mu = (\sigma_{\mathrm{H}} \, \mathrm{x} \, \mathcal{B}(\mathrm{H} \to \mu\mu))/(\sigma_{\mathrm{H}} \, \mathrm{x} \, \mathcal{B}(\mathrm{H} \to \mu\mu))_{\mathrm{SM}}$ for different values of $\mathrm{p_T(H)}$ and the different FCC-hh operating scenarios, as derived from the $H \to \mu\mu$ analysis.

A.3 Standalone results of the $H \rightarrow ZZ* \rightarrow 4\mu$ analysis

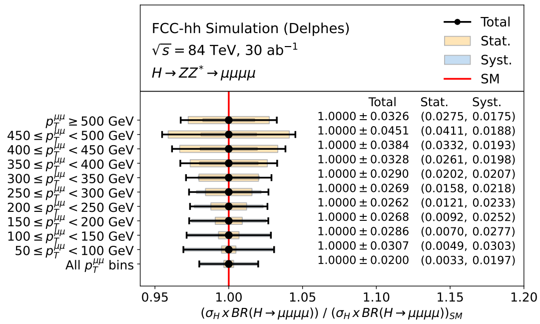

(a) FSR baseline of 84 TeV

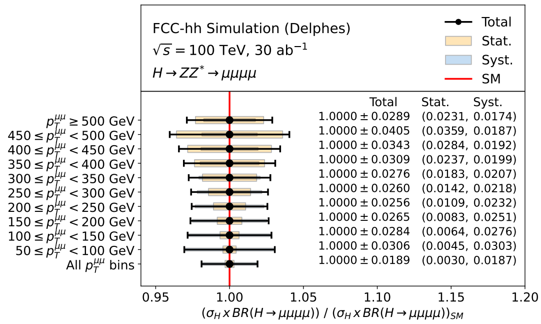

(b) CDR baseline of 100 TeV

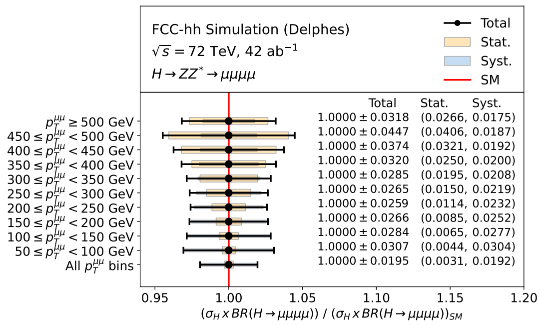

(c) F12PU scenario with 72 TeV

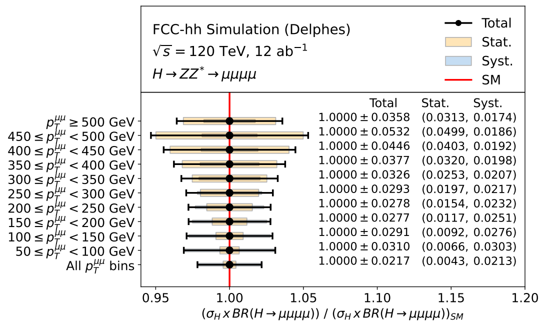

(d) F20 scenario with 120 TeV

Fig. A.3: Differential measurements of the signal strength $\mu = (\sigma_{\rm H}\,{\rm x}\,\mathcal{B}({\rm H} \rightarrow \mu\mu\mu\mu))/(\sigma_{\rm H}\,{\rm x}\,\mathcal{B}({\rm H} \rightarrow \mu\mu\mu\mu))_{\rm SM}$ for different values of $\rm p_T(H)$ and the different FCC-hh operating scenarios, as derived from the $H \rightarrow ZZ* \rightarrow 4\mu$ analysis.

Acknowledgements

This work has been partly supported by the Future Circular Collider Innovation Study (FCCIS) project, that has received funding from the European Union's Horizon 2020 research and innovation programme under grant No 951754.

References

[1] M. Selvaggi, A. Blondel, J. Eysermans. Prospects in Electroweak, Higgs and Top physics at FCC (2025). https://doi.org/10.17181/n78xk-qcv56

[2] G. Wilkinson, A. Blondel, P. Janot, C. Grojean, S. Rajagopalan. The FCC integrated programme: a physics manifesto (2025). https://doi.org/10.17181/3kaxg-ejn91

[3] A. Abada, et al., FCC Physics Opportunities: Future Circular Collider Conceptual Design Report Volume 1. Eur. Phys. J. C **79**, 474 (2019). https://doi.org/10.1140/epjc/s10052-019-6904-3

[4] A. Abada, et al., FCC-hh: The Hadron Collider: Future Circular Collider Conceptual Design Report Volume 3. Eur. Phys. J. ST **228**, 755 (2019). https://doi.org/10.1140/epjst/e2019-900087-0

[5] L. Borgonovi, et al. Higgs measurements at FCC-hh (2018). URL https://cds.cern.ch/record/2642471

[6] M. Benedikt, et al. Future Circular Collider Feasibility Study Report Volume 1: Physics and Experiments (2025). URL https://cds.cern.ch/record/2928193

[7] M. Benedikt, et al. Future Circular Collider Feasibility Study Report Volume 2: Accelerators, technical infrastructure and safety (2025). URL https://cds.cern.ch/record/2928793

[8] M. Benedikt, et al. Future Circular Collider Feasibility Study Report Volume 3: Civil Engineering, Implementation and Sustainability (2025). URL https://cds.cern.ch/record/2928194

[9] F. Zimmermann. Scenarios for the FCC-hh (2025). https://doi.org/10.5281/zenodo.14934133

[10] J. Alwall, et al., The automated computation of tree-level and next-to-leading order differential cross sections, and their matching to parton shower simulations. JHEP **07**, 079 (2014). https://doi.org/10.1007/JHEP07(2014)079. arXiv:1405.0301 [hep-ph]

[11] R.D. Ball, et al., Parton distributions for the LHC Run II. JHEP **04**, 040 (2015). https://doi.org/10.1007/JHEP04(2015)040. arXiv:1410.8849 [hep-ph]

[12] C. Bierlich, et al., A comprehensive guide to the physics and usage of PYTHIA 8.3. SciPost Phys. Codeb. **2022**, 8 (2022). https://doi.org/10.21468/SciPostPhysCodeb.8. arXiv:2203.11601 [hep-ph]

[13] M.L. Mangano, M. Moretti, F. Piccinini, M. Treccani, Matching matrix elements and shower evolution for top-pair production in hadronic collisions. JHEP **2007**(01), 013–013 (2007). URL http://dx.doi.org/10.1088/1126-6708/2007/01/013

[14] R. Contino, et al., Physics at a 100 TeV pp collider: Higgs and EW symmetry breaking studies (2016). arXiv:1606.09408 [hep-ph]

[15] M. Mangano. Physics at the FCC-hh, a 100 TeV *pp* collider (2017). URL https://cds.cern.ch/record/2270978

[16] J. de Favereau, et al., DELPHES 3, A modular framework for fast simulation of a generic collider experiment. JHEP **02**, 057 (2014). arXiv:1307.6346 [hep-ex]

[17] M. Selvaggi, B. Stapf. A Delphes parameterisation of the FCC-hh detector (2025). https://doi.org/10.17181/71pv5-tvf87

[18] P. Fernandez Declara, et al., The Key4hep turnkey software stack for future colliders. PoS **EPS-HEP2021**, 844 (2022). https://doi.org/10.22323/1.398.0844

[19] B. Francois, G. Ganis. The FCC software for PED studies (2024). https://doi.org/10.17181/8k0c4-nkr70

[20] *EDM4hep data model*. https://edm4hep.web.cern.ch/

[21] B. Stapf, J. Smiesko. List of fcc_v07 official FCC-hh production samples (2025). https://fcc-physics-events.web.cern.ch/fcc-hh/delphes/fcc-v07/ii or https://fcc-physics-events.web.cern.ch/fcc-hh/Delphesevents_fcc_v07/II.php

[22] C. Helsens, E. Perez, M. Selvaggi, V. Volkl, L. Forthomme, J. Munch Torndal. HEP-FCC/FCCAnalyses: v0.10.0 (2024). URL https://doi.org/10.5281/zenodo.13871482